Sunlight selectively modifies Maillard reaction products in a wide array of chemical reactions

Daniel Hemmler[1,2]*, Michael Gonsior[3], Leanne C. Powers[3], James W. Marshall[4], Michael Rychlik[1], Andrew J. Taylor[4], and Philippe Schmitt-Kopplin[1,2,3]*

Author affiliations

[1]*Comprehensive Foodomics Platform, Analytical Food Chemistry, Technical University Munich, Maximus-von-Imhof-Forum 2, 85354 Freising, Germany.*

[2]*Research Unit Analytical BioGeoChemistry (BGC), Helmholtz Zentrum München, Ingolstädter Landstrasse 1, 85764 Neuherberg, Germany.*

[3]*University of Maryland Center for Environmental Science, Chesapeake Biological Laboratory, Solomons, USA.*

[4]*The Waltham Centre for Pet Nutrition, Mars Petcare UK, Waltham-on-the-Wolds, Leicestershire, LE14 4RT, United Kingdom.*

Corresponding authors

Philippe Schmitt-Kopplin

Research Unit Analytical BioGeoChemistry (BGC), Helmholtz Zentrum München, Ingolstädter Landstrasse 1, 85764 Neuherberg, Germany.

Phone: +49 89 3187 3246

E-Mail: schmitt-kopplin@helmholtz-muenchen.de

Daniel Hemmler

Comprehensive Foodomics Platform, Analytical Food Chemistry, Technical University Munich, Maximus-von-Imhof-Forum 2, 85354 Freising, Germany.

Phone: +49 89 3187 2216

E-Mail: daniel.hemmler@tum.de

Summary

We report the photochemical transformation of Maillard reaction products (MRPs) under simulated sunlight into mostly unexplored photoproducts. Non-enzymatic glycation of amino acids leads to a heterogeneous class of intermediates with extreme chemical diversity, which is of particular relevance in processed and stored food products as well as in diabetic and age-related protein damage. We here reacted three amino acids (lysine, arginine, and histidine) with ribose at 100 °C for ten hours. Exposing these model systems to simulated sunlight led to a fast decay of MRPs. We studied the photo-degradation of MRPs and the formation of new compounds by fluorescence spectroscopy and non-targeted (ultra)high-resolution mass spectrometry. Photoreactions showed strong selectivity towards the degradation of electron-rich aromatic heterocycles, such as pyrroles and pyrimidines. Our data show that oxidative cleavage mechanisms dominate the formation of photoproducts. The photochemical transformations differed fundamentally from "traditional" thermal Maillard reactions and indicated a high amino acid specificity.

Introduction

Non-enzymatic browning reactions have been of great interest in food science and health. In food products, reactions between amino acids and carbonyl moieties (Maillard reaction, MR) are the main contributors to flavor and color formation.[1,2] Under physiological conditions, non-enzymatic glycation leads to irreversible protein damage (advanced glycation endproducts (AGEs)), associated with a wide range of diseases.[3] Non-enzymatic browning leads to a heterogeneous class of compounds including chromophores and fluorophores that absorb and fluoresce in the ultraviolet (UV) and visible (Vis) spectral range. Aromatic and often heterocyclic colored compounds are formed mainly in the final phase of the MR by a series of condensation reactions, many of which are only partly understood.[4–6]

During their shelf life, food products are often unavoidably exposed to sunlight. In a similar way, advanced glycation endproducts, *e.g.* in eye lenses or skin, continuously experience solar exposure. Chromophores formed as part of the advanced glycation have been suggested as possible photosensitizers producing reactive oxygen species (ROS), which lead to age-related protein photodamage. Major targets for photooxidation reactions in proteins are aromatic amino acids (tryptophan (Trp), tyrosine (Tyr), and phenylalanine (Phe)) as well as histidine (His), cysteine (Cys) and methionine (Met) residues.[7] The amino acids lysine and arginine, which are of greatest relevance in non-enzymatic glycation reactions on proteins, do not show significant absorption at >230 nm[8] and photooxidation on these amino acids has only been observed at high pH values for their unprotonated species.[9] Increased levels of AGE photosensitizers have been found in aged and diabetic lenses[10,11] as well as on long-lived skin proteins.[12] It is well accepted that the predominating mechanism involves the AGE sensitized formation of ROS, such as singlet oxygen ($^1O_2$), superoxide anion radicals ($^{\bullet}O_2^-$) and hydroxyl radicals ($^{\bullet}OH$).[13–15] Further, Wondrak and co-workers showed that AGEs can act as photosensitizers to DNA damage. Besides reactions of ROS, they also proposed other photosensitization reactions involved in phototoxicity mechanisms.[16]

Because of the chemical nature of reducing sugars, the initial condensation with amine compounds and subsequent downstream reactions lead to a wide range of compounds with carbonyl functional groups, including dicarbonyl moieties and α-hydroxy ketones.[2,17] When irradiated with UV-B light, carbonyl functional groups can form acyl radicals in aqueous solutions, predominantly by Norrish-type-I photofragmentation reactions.[18–20] The α-cleavage and subsequent decarbonylation is about an order of magnitude faster for α-hydroxy ketones compared to their

alkyl counterparts.[19] Although the nature of compound classes formed during the MR suggests a strong photochemical reactivity, to date, the effect of solar radiation on the direct chemical alteration of MRPs is only partially explored. Bohart and Carson were the first to report decolorization in glucose-glycine Maillard model systems when they were exposed to illumination under oxygen in the laboratory.[21] Later, Kessel and co-workers showed that UVA radiation readily degrades purified argpyrimidine.[22]

Here we report photochemical effects on MRPs using holistic non-targeted analysis. More precisely, we exposed reaction products, initially formed by heating different amino acid-ribose mixtures at 100 °C for ten hours, to a simulated solar spectrum. Chemical changes were analyzed by optical spectroscopy and (ultra)high resolution mass spectrometry. We focus on three different amino acids (lysine, arginine, and histidine), the MRPs of which provide abundant chromophores. While lysine and arginine are the main contributors to non-enzymatic glycation reactions in foods and on proteins under physiological conditions, histidine is among the major protein residues for ROS driven cellular photodamage. Ribose has been chosen because of its high reactivity, readily leading to a large number of MRPs upon thermal processing.

Results and discussion

Effect of simulated solar irradiation on absorption and fluorescent properties of Maillard Reaction Products

Excitation emission matrix measurements of MRPs and during photo-degradation experiments. After an induction period, heating reducing sugars in the presence of amino acids leads to the formation of chromophores and fluorophores.[23] Among the proteinogenic amino acids, especially those with basic functional side chains show significant color formation in unbuffered solutions while not being affected by amino acid autofluorescence.[24] After heating three different model systems (ribose-lysine, ribose-arginine, and ribose-histidine) for ten hours at 100°C excitation-emission-matrices (EEM) were constructed from fluorescence measurements (Fig. 1a-c). Fluorescence intensities and excitation/emission wavelengths strongly depended on the amino acid precursor. Interestingly, ribose-histidine showed the most complex fluorescence behavior with at least two major emitting regions indicating multiple chemical structures and moieties participating in the overall fluorescence behavior. In the ribose-lysine and -arginine model systems we observed dominating fluorescence peaks with emission maxima at 440 nm (excitation: $\leq$ 245 nm and 350 nm) and 400 nm (excitation: $\leq$ 245 nm and 320 nm), respectively. Only a few fluorescent MRPs have been previously fully characterized. Most of them were isolated from model systems containing the amino acids lysine and arginine[25]. Many of the studied fluorescent MRPs are involved in the crosslinking of proteins and are used as important markers in the formation of AGEs. Pentodilysine (LM-1), a fluorescent molecule cross-linking lysine residues, has excitation/emission wavelengths that would match the dominating fluorescence peak in the ribose-lysine model-system (Fig. 1a).[26,27] In a similar way, argpyrimidine shows excitation/emission corresponding to the major peak found in the ribose-arginine model system (Fig. 1b).[28] While pentodilysine can be formed directly from ribose and lysine, argpyrimidine is formed from arginine and methylglyoxal.[27,28] Fluorophores formed in the Maillard reaction by other amino acids than lysine and arginine have received only minor attention[25] even though some studies support that fluorescent MRPs may be related to the formation of brown pigments.[24]

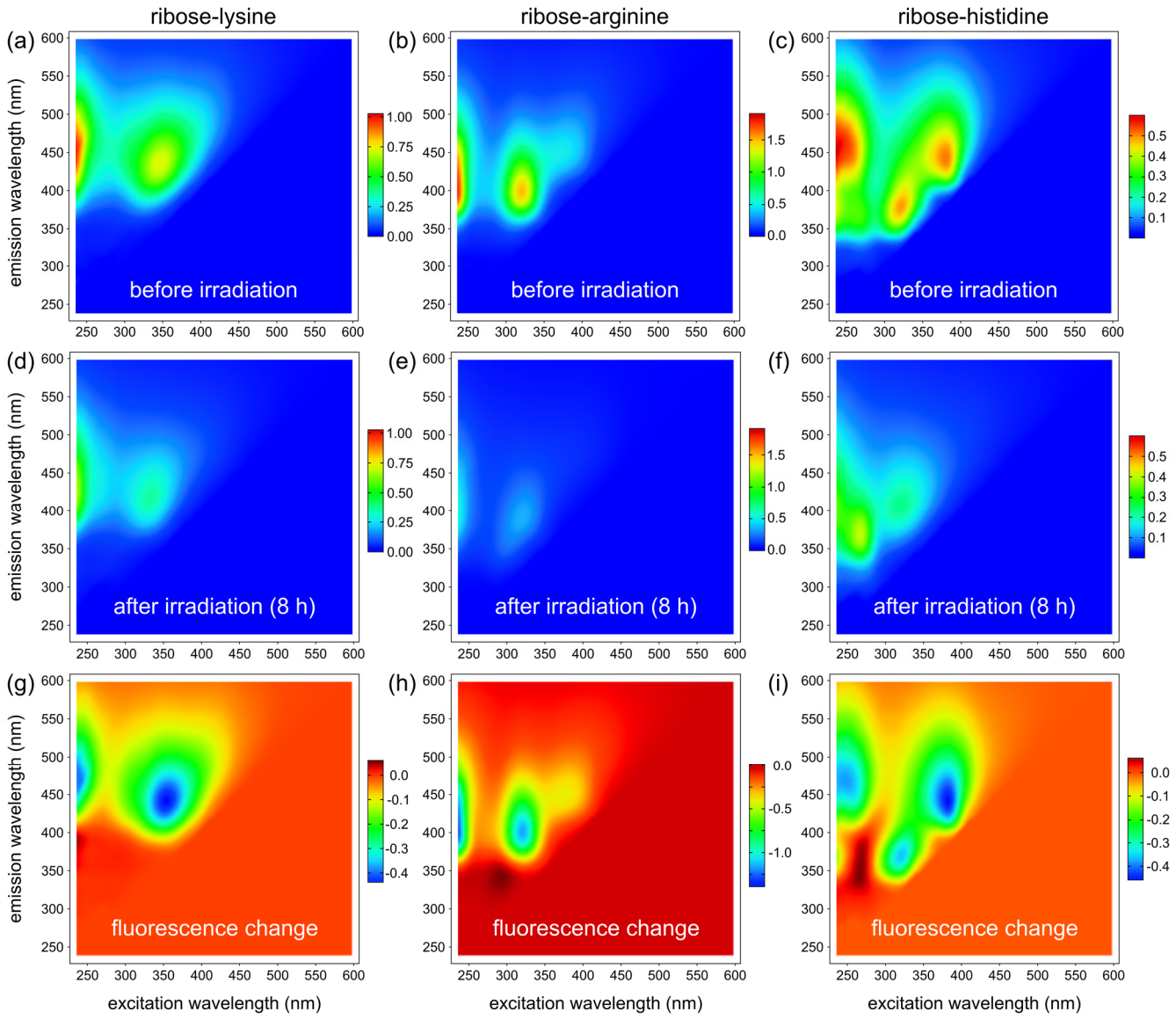

Figure 1. Photolytic degradation of MRPs in three model systems (ribose-lysine, -arginine, and –histidine) heated for ten hours at 100 °C. Excitation-emission-matrices retrieved from diluted model systems (1:800 *v/v* in H_2O) (a-c) before irradiation and (d-f) after solar irradiation for 8 h. (g-i) Changes in fluorescence intensity after an irradiation time of 8 h. All fluorescence intensity values are expressed in quinine sulfate units (ppm).

The same model systems (ribose-lysine, -arginine, and –histidine) were then exposed to solar irradiation to initiate photo-decomposition (e.g. photobleaching and photo-transformations). Upon solar irradiation, we observed a fast decay in fluorescence intensities in all model systems (Fig. 1d-i). Besides the decrease in fluorescence, however, the EEM maps in Fig. 1g-i also indicate formation of new fluorescent compounds, which were formed during the photolysis or which have been quenched by other compounds prior to irradiation. Parallel factor analysis (PARAFAC) was used to decompose fluorescence spectra into distinct statistical components.[29] For all three model systems, four component PARAFAC models could be developed and split-half validated. Besides the above-

mentioned characteristic spectral regions, the PARAFAC models give evidence for the existence of additional fluorophores, even though with lower quantum yields (Fig. 2 and Table 1). For all model systems, three components were retrieved which showed a decrease in fluorescence and one fluorescent component which increased over time, respectively. These components (Lys: C2, Arg: C2, His: C1) show very different excitation/emission positions and different Stoke's shifts between the model systems indicating different chemical structures and fluorescent moieties, respectively. In the ribose-lysine model system, the increase of C2 showed remarkable correlation to the decreasing fluorescence of C3 and C4. Hence, C2 may be formed by photochemical reactions of C3 and/or C4, or these fluorophores may have quenched the fluorescence of C2 before irradiation. A similar correlation could be found for C2 and C3/C4 in the ribose-arginine reaction system. Very similar fluorescence peaks further indicate the possibility of similar substructures (fluorophoric groups) between C4 of the ribose-lysine and C4 of the ribose-arginine systems. In general, the photo kinetics derived from the PARAFAC components are very similar between the lysine and arginine reaction systems. By comparison, fluorophores degraded and potentially formed in the ribose-histidine model system behaved differently. For example, the increasing component (C1) showed a nearly linear increase in fluorescence over the entire irradiation period indicating zero order photochemical synthesis.

Table 1. Fluorescence local maxima obtained by EEM-PARAFAC analysis.

component	lysine	arginine	histidine
C1: Ex | Em	350 | 440 nm	320 | 400 nm	265 | 365 nm
C2: Ex | Em	270 | 430 nm	295 | 350 nm	330 | 420 nm
C3: Ex | Em	330 | 395 nm	355 | 430 nm	245 | 470 nm 380 | 470 nm
C4: Ex | Em	240 | 485 nm 395 | 485 nm	245 | 480 nm 395 | 480 nm	325 | 370 nm

Absorbance measurements. After heating the ribose-amino acid mixtures for ten hours at 100 °C, we found maximum absorbance at 265 nm in the ribose-lysine and –histidine mixture (Fig. 3). The arginine reaction system showed maximum absorbance < 240 nm but indicated a second maximum at about 300 nm. Irradiation of the samples led to an exponential decrease in absorbance with maximum decrease found at 336 nm, 327 nm, and 294 nm for the ribose-lysine, -arginine, and -histidine model system, respectively (Fig. 3). The discrete maxima indicate a selectivity of photochemical reactions rather than random degradation of all chromophores absorbing in

the irradiated energy range. A red-shifted shoulder in Fig. 3c (ribose-histidine model system) indicated an underlying curve with a second maximum decrease in absorbance at approx. 340 nm, which was in the range found for the ribose-lysine and ribose-arginine model systems, and could represent degradation reactions on chromophoric groups, similar to those in the lysine and arginine systems. The relative degradation rates of the two maxima found at 294 nm and 340 nm in the ribose-histidine model system were different. Especially at the beginning of the irradiation process, degradation rates at 340 nm were faster than for chromophores showing greatest changes at 294 nm (Fig. 3c). This suggests at least two different groups of chromophores and potentially different degradation mechanisms.

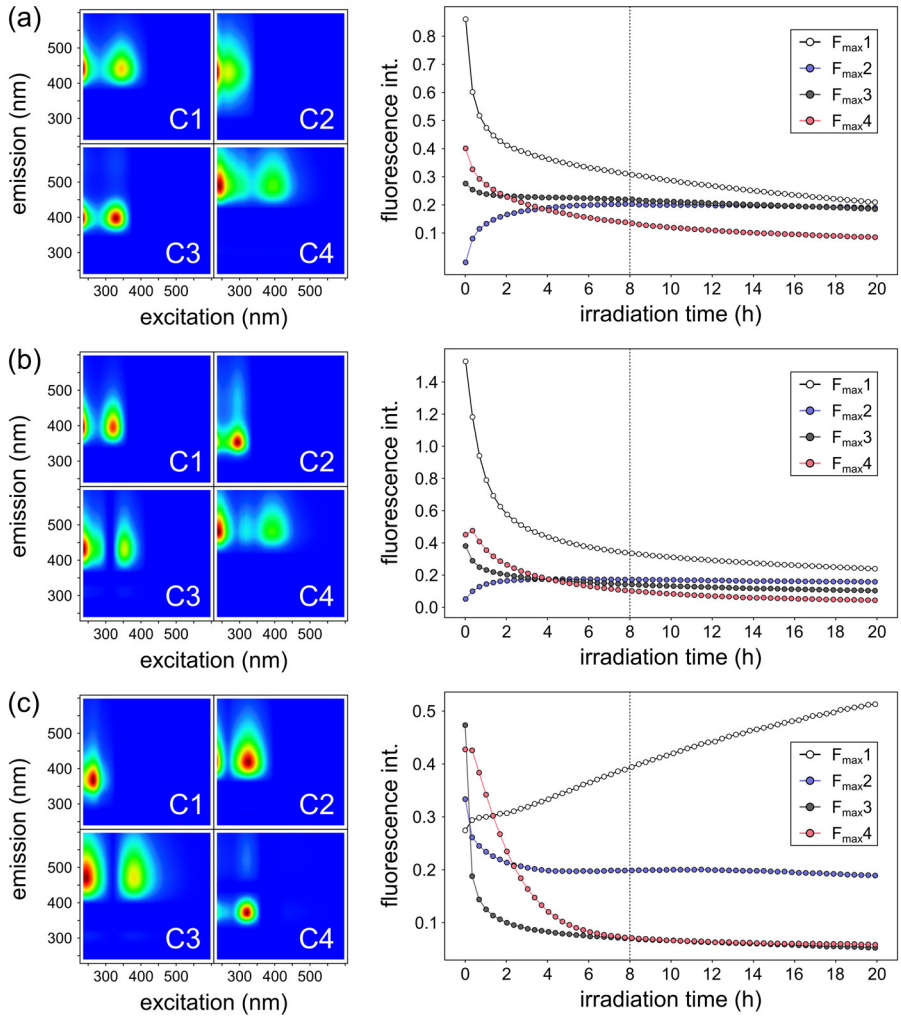

Figure 2. Four component EEM-PARAFAC models obtained from EEM measurements. (a) Ribose-lysine, (b) ribose-arginine, and (c) ribose-histidine model systems. All model systems were irradiated for 20 h. EEM spectra were recorded every 20 min.

Holistic characterization of photosensitive MRPs

We additionally irradiated larger amounts of sample in a suntester solar-simulation system equipped with a xenon arc lamp, also simulating the solar spectrum. Irradiation was performed for four and eight hours while the temperature was maintained at 25 °C. Control samples, which were protected from light exposure, were also placed in the suntester system for four and eight hours. Subsequently, we analyzed the samples by direct-infusion Fourier transform ion cyclotron mass spectrometry (FT-ICR-MS) and Tandem-column-LC-MS/MS, which combines hydrophilic interaction chromatography (HILIC) and reversed-phase (RP) liquid chromatography (LC) in a single chromatographic run.[30] Direct-Infusion FT-ICR-MS allows a highly sensitive and holistic non-targeted screening of complex samples on the level of accurate molecular formulae.[31] To provide further data for comparison, LC-MS/MS was used to monitor irradiation effects for specific candidate compounds and to study effects on the chemical structures. Principal Component Analysis (PCA) of the obtained FT-ICR-MS raw data could clearly separate irradiated model systems from controls on PC1 (exemplarily shown for the ribose-histidine model in Fig. S1). Samples irradiated for four hours could also be distinguished from samples exposed to sunlight for eight hours by PC2. Moreover, we could not observe a difference between the control samples kept for four and eight hours in the suntester (while protected from light exposure) and freshly prepared model systems. This indicates that no significant thermal or time effects on the formation of new MRPs took place during irradiation experiments.

Photochemical degradation of MRPs. In total, we could detect 1446, 1945, and 2066 monoisotopic signals in unirradiated ribose-histidine, -lysine, and -arginine model systems, respectively, using FT-ICR-MS. Upon solar irradiation, we observed the largest changes in the ribose-histidine model system. Here, 391 elemental compositions (20%) showed a significant decrease in peak intensities after an irradiation time of eight hours ($p < 0.01$ and log2FC < -1 in both replicate experiments) (Fig. 4). By comparison, in ribose-lysine and –arginine model systems irradiation led to 42 (2.2%) and 88 (4.3%) elemental compositions, which showed a significant decrease in *m/z* ion intensities (Fig. S2-S3).

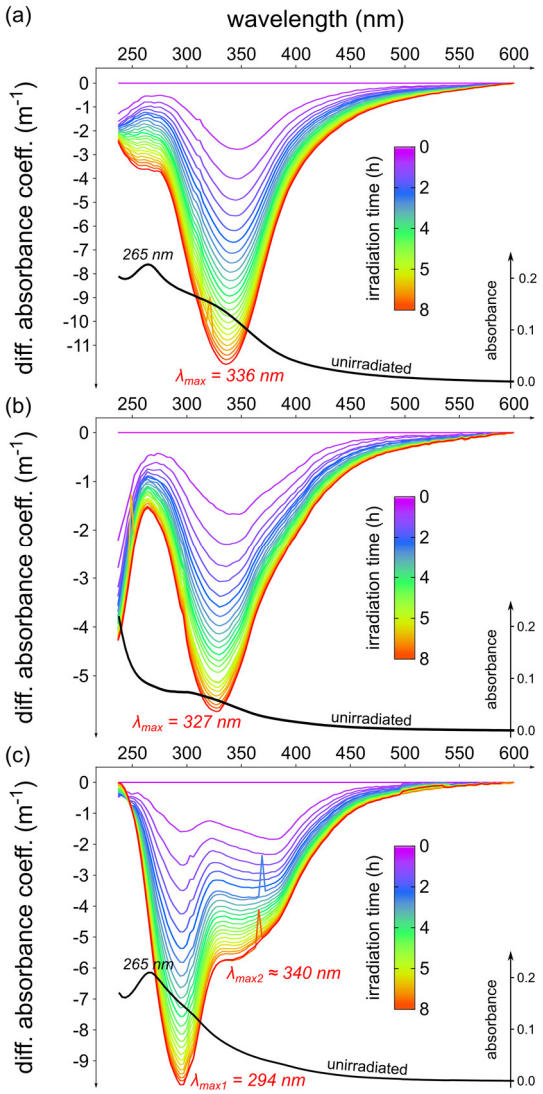

Figure 3. Changes in the absorption spectra upon irradiation. Differential absorbance spectra of (a) ribose-lysine, (b) ribose-arginine, and (c) ribose-histidine model systems irradiated for eight hours. UV-Vis spectra were recorded every 20 minutes simultaneously with EEMs presented above. Embedded black curves represent UV-Vis absorption spectra of unirradiated model systems (10 h, 100° C), respectively.

Photooxidation of MRPs by singlet oxygen. Histidine residues are well known to easily undergo photooxidation reactions.[7,32,33] However, direct light absorption by the imidazole function is not the major mechanism.[33] In oxygen-rich atmospheres histidine photooxidation mainly occurs via Type II photo reactions.[34] In a Type II reaction, the energy absorbed by a sensitizer is transferred onto ground state molecular oxygen to produce singlet oxygen ($^1O_2$) and to a lesser extent other ROS.[13] Singlet oxygen then may form unstable endoperoxide intermediates on imidazole residues, which further decompose into a complex mixture of as yet mostly unknown products.[35,36] Among the proteinogenic amino acids, only Trp, Tyr, Phe, His, Cys, and Met show noteworthy rate constants in the reaction with $^1O_2$ with the highest values found for histidine oxidation,[37,38] which might explain the greater number of photolabile MRPs in the ribose-histidine model compared to the two other model systems investigated.

Nevertheless, formation of $^1O_2$, and subsequent reactions of MRPs with $^1O_2$ may also play a role in the ribose-lysine and arginine model systems, particularly due to photosensitizers that can be produced in the course of the MR. We could detect significantly elevated levels of urea and asparagine in the irradiated histidine model systems (Fig. S4), which are formed in the decomposition of histidine via $^1O_2$.[36,39] Assuming that urea and asparagine are exclusively formed from photooxidation reactions, quantification (by LC-MS) of the formed urea and asparagine, suggested up to 0.06 – 0.09% and 0.002% of the initial histidine amount being transferred into urea and asparagine, respectively (Fig. S4). While urea can also be formed by α-NH_2-substituted histidines, asparagine can only be formed by degradation of the free amino acid.[36]

Several studies showed that rate constants for $^1O_2$-photoxygenation reactions on α-NH_2-substituted histidines are in the same order of magnitude as for the free amino acid indicating that the major target for photooxidation is the imidazole group of histidine.[36,40,41] Notwithstanding this, many of the compositions that remained unchanged after irradiation, such as the Amadori rearrangement product (ARP) and other MRPs of the initial and intermediate phase (Fig. 5), also contain intact histidine residues. Furthermore, when screening for imidazole fragments in MS/MS data, we could not observe a preferred degradation selectivity when MRPs contained intact imidazole groups (Fig. S5). The MS/MS spectra further revealed that most of the molecules formed upon irradiation still contained intact imidazole functions (Fig. S5). Conclusively, imidazoles cannot be the dominating targets for photooxidation reactions but the nature of substituents at the α-NH_2 position seems to play a decisive role in the reactivity towards photons. It has been shown that the pH in aqueous solutions strongly affects the $^1O_2$ oxygenation of histidine residues, indicating that oxygenation mainly occurs on unprotonated imidazole residues.[42,43] The initial pH of the histidine model systems used in this study was equal to the pKa value of the histidine side chain (pH 6). Within eight hours of irradiation, the pH value had dropped exponentially to about pH 5.5 (Table S1-S2). Consequently, the amount of unprotonated imidazoles in the model systems strongly decreased and it is conceivable that other moieties predominate in the photochemical degradation of histidine derived MRPs.

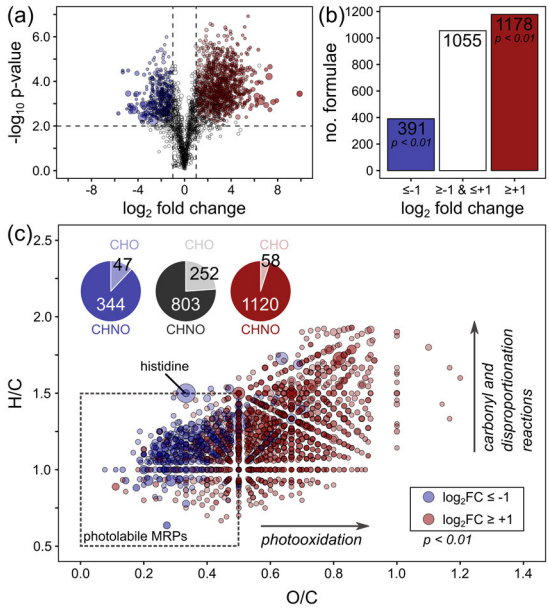

Figure 4. Effect of solar irradiation on elemental compositions of ribose-histidine MRPs. Model systems were irradiated for eight hours and compared to unirradiated control samples. Irradiation experiments were performed in duplicate. Each sample then was analyzed by FT-ICR-MS in triplicate injections (N = 2 × 3). Peak intensities of all features found in irradiated samples were compared to the same features in the unirradiated control samples by Student's t-Test (n = 3): Features, which showed a significant decrease in peak intensities in both independent irradiation experiments are colored in blue. Features, which showed a significant increase or were newly formed upon irradiation are highlighted in red, respectively. (a) Volcano plot. (b) Number of molecular formulae showing significant changes in peak intensities. (c) Van Krevelen diagram of all significantly affected molecular formulae. Pie charts illustrate the reduced occurrence of nitrogen-free (CHO) MRPs in photochemical reactions. Black pie chart represents elemental compositions, which did not show a significant change in peak intensities upon irradiation.

Photochemical selectivity. Interestingly, molecular formulae of the photochemically degraded species cover a discrete area in the Van Krevelen space (Fig. 4c, Fig. S2c, and Fig. S3c). The majority of degraded compounds have small H/C and O/C ratios, which are characteristic of unsaturated and aromatic compounds. In all model systems, most of the photochemically degraded compounds were characterized by an O/C-ratio ≤ 0.5 and an H/C-ratio ≤ 1.5. Even though the different amino acids led to the formation of very different, largely amino acid specific MRPs (Fig. S6), this "photolabile area" was the same for all model systems. In the photolabile area, we reproducibly found 617, 611, and 851 molecular formulae, accounting for 34%, 21% and 57% of the total peak intensity, in the ribose-lysine, -arginine, and -histidine model systems, respectively. This somewhat higher number and higher molar amounts (estimated as relative peak intensities) found in the ribose-histidine MR may explain to a certain extent the higher number of degraded MRPs found in the histidine MR.

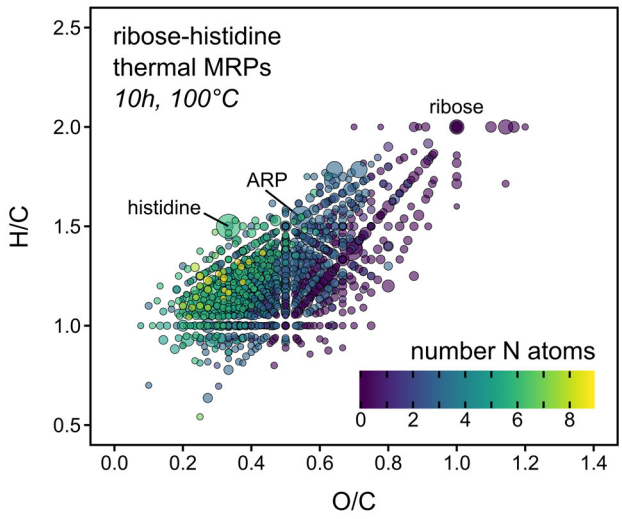

Figure 5 Van Krevelen diagram of all molecular formulae reproducibly found in two independent replicate experiments (each analyzed in triplicate) after heating a ribose-histidine model system for ten hours at 100 °C. Color indicates the number of nitrogen atoms in the formulae. Scaling is relative to the average peak intensity recorded by FT-ICR-MS.

Several studies reported significantly greater antioxidant activity of MRPs formed from histidine compared to other amino acids.[44,45] Indeed, antioxidants exhibit compositional characteristics (H/C and O/C-ratios; Fig. S7) similar to the compounds found in the photolabile area shown in Fig. 4. Hence, increased active oxygen and radical scavenging activity[46,47] found for these MRPs may also play a role in the photochemical selectivity and the greater number of photo-modified MRPs in the histidine model system.

Only a few AGE markers, which can be formed in the ribose-lysine and –arginine MR, have been described previously.[48] We could identify seven compounds in our LC-MS/MS data (Fig. 6), and we used fragmentation spectra to substantiate chemical structures (Fig. S8-S9). Among the seven identified candidates, only formyline[49] and argpyrimidine[28] showed significant degradation ($log2FC < -1$ and $p < 0.01$, Student's t-Test ($n = 3$)) after an irradiation time of eight hours in both irradiation experiments. Heterocyclic aromatic groups (pyrrole and pyrimidine) characterize these markers. In the two imidazole derivatives, GOLD and MOLD[50], both nitrogen atoms are substituted leading to a positive charge and therefore a reduced electron density in the aromatic ring structure, similar to protonated histidine residues. This indicates a selectivity of photochemical degradation reactions, towards the degradation of electron-rich aromatic heterocycles, which are preferentially formed in the final phase of the MR and often responsible for the characteristic browning (melanoidins).[1,51]

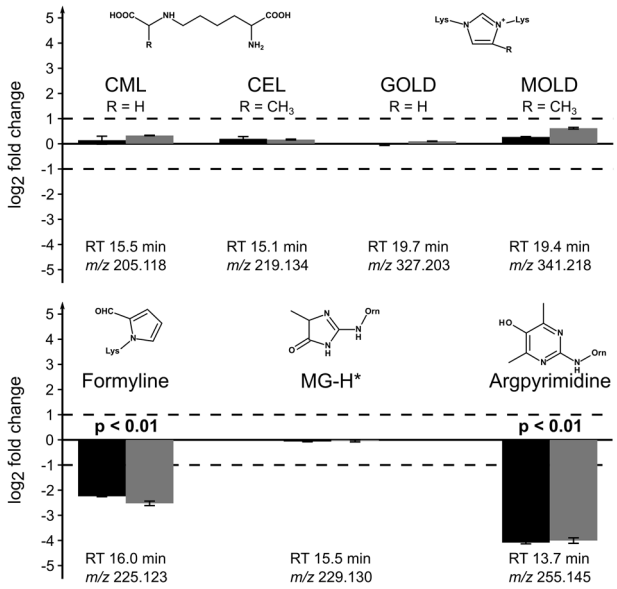

Figure 6. LC-MS/MS analysis of known AGEs and MRPs that can be formed in the ribose-lysine and –arginine Maillard reaction, respectively. Log2 fold changes represent the changes in peak intensities between irradiated (8 h) and unirradiated control samples. Two independent irradiation experiments (experiment A: dark grey, experiment B: grey) were carried out. Each experiment was analyzed in triplicate injections by LC-MS/MS.

Photo-induced formation of MRPs. In all model systems, we found far more compounds, which were produced upon solar-simulated irradiation than MRPs that were degraded. More precisely, analysis of the ribose-histidine model system showed 1178 compounds after irradiation, which significantly increased in their *m/z* ion intensities ($log2FC > 1$, $p < 0.01$, Student's t-Test ($n = 3$)) or were newly formed (Fig. 4). By comparison, the ribose-lysine and arginine model systems showed 167 and 525 elemental compositions increasing in intensity after an irradiation time of eight hours, respectively (Fig. S2-S3). Compared to the degraded MRPs, the photochemically formed products showed a clear shift towards higher O/C-ratios indicating that oxidation reactions are involved in the photochemical modification of MRPs. While most of the photooxidation products can be formed by successive oxidation of double bonds ($O/C > 0.5$ and $H/C <= 1.5$), we also found a considerable number of photoproducts with an H/C-ratio greater than 1.5 (Fig. 4c). These reaction products might be formed by disproportionation reactions or by reactions on carbonyl groups, such as hydroxyl carbonyls or deoxyosones, with nucleophilic components of the system. Many of the degraded MRPs in the photolabile area may also serve as good scavengers for (hydroxy)-acyl radicals formed by Norrish-type reactions during the irradiation process.[18] In general, these type of photoproducts have similar elemental compositions as thermally formed MRPs found in the initial and intermediate phase of the MR (Fig. 5).

We further studied the behavior of different compositional descriptors, which can be retrieved from the computed molecular formulae (Fig. 7 and Fig. S10-S11). Interestingly, all model systems showed similar behavior, which can be summarized as follows:

(i) MRPs with a higher molecular weight and a larger number of carbon atoms preferably undergo photolytic reactions. By comparison, photochemical products tend to be smaller molecules with a reduced number of carbon atoms (Fig. 7a), indicating that cleavage mechanisms are likely to be involved in photochemical reactions on MRPs.

(ii) Upon photolytic reactions, the number of oxygen atoms per molecule increased on average by 1.5 oxygen atoms per molecule (Fig. 7b). Together with the increase in the average carbon oxidation state (Fig. 7f), it can be concluded that exogenous ROS, such as $^1O_2$ or hydroxyl radicals, must play a key role in the photochemical reaction mechanisms.

(iii) Photosensitive MRPs have a higher number of double bond equivalents (sum of double bonds and rings) per carbon atom (DBE/C) than MRPs that are stable towards light exposure (Fig. 7e). However, we could not observe a noticeable difference between the DBE/C-values of the degraded and the photochemically produced compounds. For example, after cleavage of a carbon-carbon double bond each of the two carbon atoms must still contain a double bond to maintain the DBE/C value. Because the average carbon oxidation state of the photolysis products tends to have higher values than that of the other MRPs, it is likely that double bonds undergo photooxidative cleavage reactions leading to the formation of carbonyl moieties such as aldehydes or carboxylic acids. A decrease of the pH-value during the irradiation experiments (Table S1-S2) further supports the formation of carboxylic acids in the course of photolysis.

(iv) Photolabile MRPs tend to be nitrogen rich compounds (Fig. 7d). When irradiated, the number of nitrogen atoms in the reaction products decreased. This substantiates photochemical targets, such as nitrogen containing heterocyclic structures or Schiff bases that might undergo oxidative degradation similar to the Karstens and Rossbach mechanism.[52]

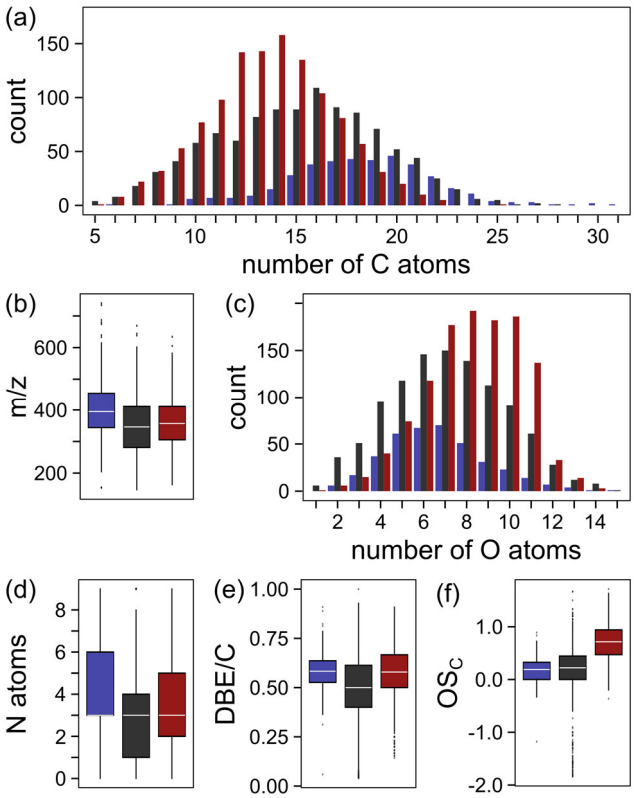

Figure 7. Overview of compositional descriptors retrieved for the ribose-histidine model system after molecular formulae computation from FT-ICR-MS data. Bar charts are grouped into features, which showed a significant decrease (blue; log2FC < -1 and p < 0.01, Student's t-Test (n = 3)) and significant increase (red; log2FC > 1 and p < 0.01, Student's t-Test (n = 3)) in peak intensities in both independent irradiation experiments, respectively. Features that did not show a significant change in peak intensities after an irradiation time of eight hours are colored in black. Represented descriptors are (a) number of carbon atoms per formula, (b) measured *m/z*-values, (c) number of oxygen atoms per formula, (d) number of nitrogen atoms per formula, (e) average number of double bond equivalents per carbon atom, and (f) average carbon oxidation state.

Amino acid-specific photochemical reactions and their orthogonality to thermal reactions. Non-targeted analysis aims to comprehensively investigate a sample's chemical composition. Although we are unlikely to be able to resolve and detect the entire chemistry of very complex samples, we can potentially find many precursor-product pairs in the mass spectra obtained from non-targeted experiments of reaction systems. The mass difference between a potential reaction precursor and product can provide information about their net chemical transformation.[53,54] Even though not all mass differences correspond to a real chemical transformation, they can provide useful information about the compositional connectivity between the observed reaction products.[55] We computed all mass differences between all monoisotopic ions observed in the FT-ICR mass spectra and used their relative incidences to elucidate meaningful mass differences (Fig. 8). For example, an incidence rate of 54%, as found for the mass difference 18.010565 Da (compositional equivalent: ± H_2O) in the unirradiated ribose-histidine

model system (Fig. 8), means that 54% of all monoisotopic ion signals in the spectra can be connected to another signal by this mass difference.

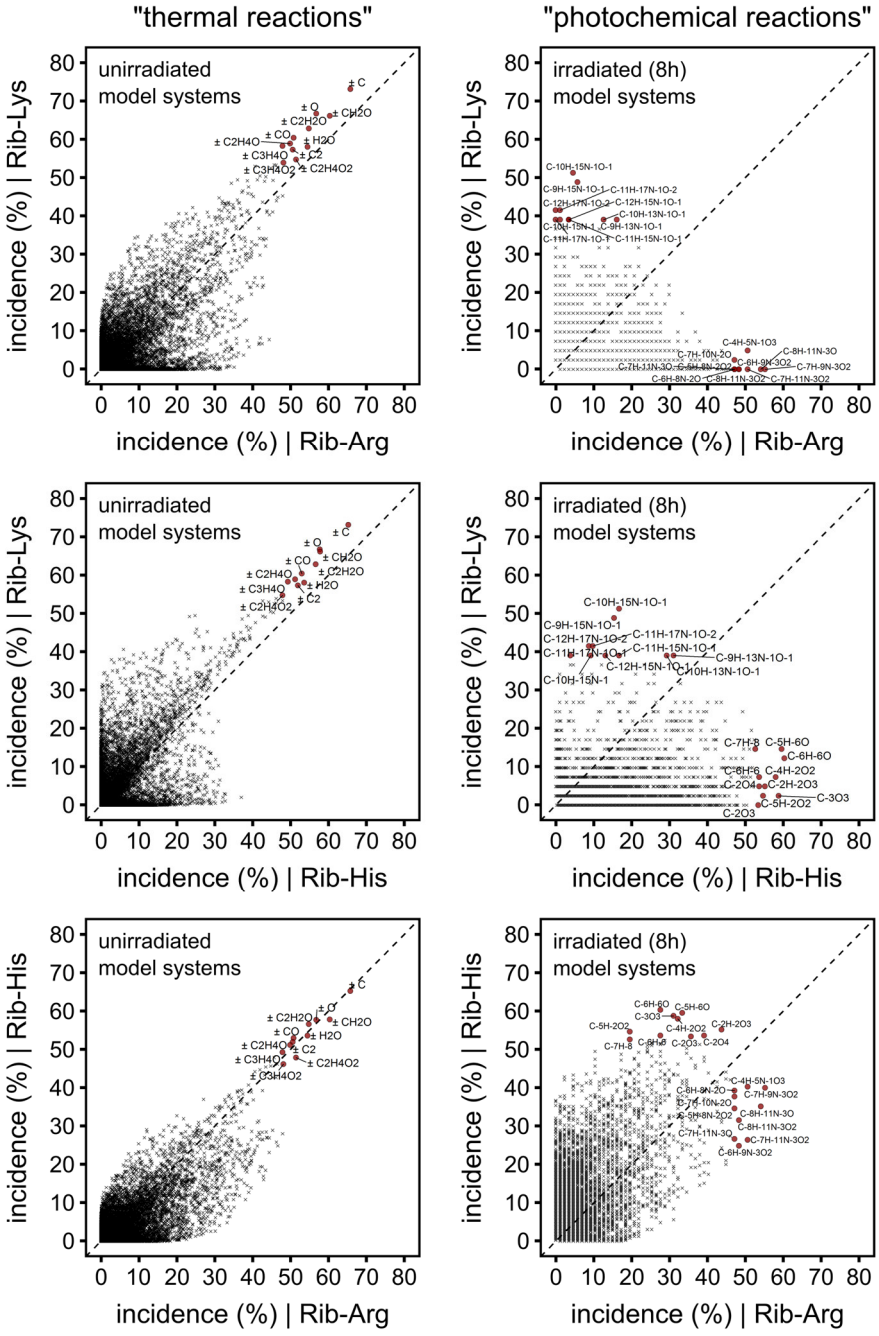

Figure 8. Pairwise comparison of mass difference incidences. Incidence rates were computed from all recorded mass differences in the mass spectra of thermally synthesized MRPs (left panel) and photochemically synthesized products (right panel). The top ten of the most frequently occurring mass differences were assigned to their element compositional equivalents representing possible net chemical transformations. Incidences represent the relative probability by which a monoisotopic signal in the mass spectrum can be linked to another monoisotopic signal with a given mass difference md_i.

Pairwise comparison of the different unirradiated control model systems showed good correlation of mass differences, especially those with high incidence rates, indicating very similar chemical reactions in the thermal formation of MRPs. These mass differences involved chemical transformations, such as (de)hydration (± H_2O) and oxidation/reduction (± O), which are known to play a crucial role in the thermal synthesis of MRPs. This data agrees with our recent study, which showed that different amino acid precursors follow consistent reactivity behavior, even though the different amino acid precursors lead to very different chemical compositions.[56] By comparison, when comparing mass differences, which were exclusively found between degraded MRPs ("photo-precursors") and compounds formed upon irradiation ("photo-products") we received a completely different picture (Fig. 8). Firstly, compared to the thermally formed MRPs, we observed poor correlation of reactivity patterns between the different model systems, indicating photochemical reactions of MRPs are very specific to the parent amino acids. Secondly, net chemical transformations that are dominating the MR in thermal processing seem to play only a minor role in the photochemical reactions of the MRPs. It is worth noting, that intermediate reactions, which do not lead to stable molecules that can be detected by MS, are not considered with this approach. Conclusively, while major chemical reactions in the thermal synthesis of MRPs are very consistent and independent of the amino acid precursor, the same systems show strong amino acid specificity in the photochemical degradation of MRPs.

Conclusions

We studied the effects of solar-simulated radiation on the modification of MRPs, formed in a typical non-enzymatic browning reaction at moderate temperature (100 °C). Upon photon absorption, hundreds of MRPs readily underwent degradation reactions leading to a complex mixture of newly formed photoproducts. Our data provides evidence for a strong selectivity of photo-degradation reactions, mainly towards electron-rich and nitrogen-containing heterocycles, which are preferentially formed in the advanced and final phase of the Maillard reaction. Photoreactions on these structures break down the molecules into smaller but strongly oxidized compounds. While the "traditional" (thermal) synthesis of amino acid glycation products follows general chemical reactions, such as dehydration, carbonyl cleavage and redox reactions, photoreactions are a lot more diverse and show strong amino acid specificity. This fundamental study is of special importance in the shelf-life of foods, phototoxicity mechanisms in diabetic and aged tissues and may, under certain conditions, also play a role in prebiotic molecular

synthesis. Lack of current comprehensive database information on MRPs and photochemical products did not allow identification of structures, but also suggests a great pool of as yet unexplored chemical compounds, which need detailed characterization in future studies. Studies on purified reaction products may help to understand some specific photo-degradation mechanisms. However, it must be taken into consideration that many of the formed photoproducts are likely to be produced only in a complex interplay of reactive intermediates and products. Hence, further improvements in holistic approaches are required to gain better understanding.

Experimental procedures

Chemicals and reagents

L-Arginine (≥98%), L-asparagine (>99%), L-histidine (98%), L-lysine (>98%), and D-(-)-ribose (98%) were purchased from Sigma-Aldrich (Steinheim, Germany). Urea (100%) was obtained from Beckmann Coulter (Krefeld, Germany). LC-MS grade methanol and acetonitrile were purchased from Merck (Darmstadt, Germany). Formic acid (LC-MS grade) and ammonium formate (10 M stock solution) were obtained from Sigma-Aldrich (Steinheim, Germany). MilliQ-purified water (18.2 MΩ; Millipore, Germany) was used throughout the experiments.

Maillard model systems

Equimolar mixtures of ribose and amino acids (0.1 mol L^{-1} respectively) were prepared in MilliQ-purified water. 1 mL of each mixture was heated in closed glass vials as recently described at 100 °C for ten hours[31]. Model systems were stored at -20 °C until usage.

Irradiation experiments

All Maillard model systems were diluted 1:800 (*v/v*) with MilliQ-purified water prior to irradiation. Aliquots of the model systems were irradiated in a custom-built photolysis system, as described in detail elsewhere.[57,58] Irradiation experiments were performed for 20 h with a 1000 W Xe arc lamp equipped with an air mass filter (AM 1.5). Before each irradiation experiment, the lamp intensity was controlled to ensure that the irradiated sample receives a radiation dose, which is equivalent to the sun at Earth's surface (45° north, midsummer, at noon). The temperature

was controlled at 25 °C using Peltier units and a circulating water bath. The pH value was monitored throughout the irradiation process (Table S1).

For subsequent FT-ICR-MS and LC-MS/MS analysis, larger sample amounts were irradiated, with the same dilution as above (1:800 (*v/v*)), in quartz vessels in a Suntest CPS system (Heraeus, Hanau, Germany) equipped with an NXE xenon lamp (Atlas Material Testing Technology, Gelnhausen, Germany) for four and eight hours. The temperature was maintained at 25 °C using an air conditioning unit and the pH was recorded before and after irradiation (Table S2), respectively. Additionally, control samples in lightproof vessels were placed under the xenon lamp. All samples were irradiated in two independent experiments (n = 2).

Excitation emission matrix fluorescence

Online EEM measurements during the irradiation were performed every 20 min using a 4 × 10 mm flow cell and an Aqualog spectrofluorometer (Horiba Instruments, New Jersey, USA). Excitation ranged from 230 to 600 nm and emission was recorded between 211 to 617 nm. All fluorescence spectra were corrected for scatter and inner filter effects. Normalization to a 1 mg L^{-1} quinine sulfate standard (Starna reference material RM-QS00, 1.28×10^{-6} mol L^{-1}) was used to express all fluorescence intensities in quinine sulfate units (ppm). Independently for each irradiated model system, PARAFAC models were built using the drEEM toolbox for MATLAB.[29] The data best fitted four-component PARAFAC models, which were split-half validated, explaining 99.8%, 99.8%, and 99.7% of the spectral variance in the ribose-lysine, -arginine, and -histidine model system, respectively.

FT-ICR-MS analysis

All irradiated Maillard model systems were further diluted with methanol to achieve a final dilution of 1:2500 (*v/v*) immediately prior to FT-ICR-MS analysis. Each sample was analyzed in three independent injections (n = 2 × 3 = 6 MS measurements). Direct-infusion FT-ICR mass spectra were acquired with a 12 T Bruker Solarix mass spectrometer (Bruker Daltonics, Bremen, Germany). Samples were infused with a flow rate of 2 µL min^{-1} into an APOLLO II electrospray source operated in negative ionization mode. Ion source settings and spectra calibration were the same as recently described.[31] Spectra were acquired with a time-domain of 4 megawords and 300 scans were accumulated within a mass range of *m/z* 123 to 1000.

Peaks with a signal-to-noise ratio of at least eight were exported to mass lists. Data prefiltering was used to remove FT artifacts[59], features with unusual mass defects and ^{13}C isotope signals. Peaks were then aligned into a matrix containing averaged *m/z*-values and corresponding peak intensities allowing a maximum alignment window of 1 ppm.[60] Only those *m/z*-values were retained in the matrix, which were reproducibly found in all three replicate injections of at least one sample. Zero values in the matrix then were replaced by the recorded absolute intensity values found in the raw spectra at that *m/z*-value, respectively. Finally, molecular formulae were computed for all averaged *m/z*-values as recently described.[56]

Tandem HILIC-RP LC-MS/MS

16 ml aliquots of the irradiated samples were lyophilized until dryness and immediately reconstituted in 200 µl of an aqueous solution containing 2% acetonitrile prior to LC-MS/MS analysis. Instrumental setup and chromatographic conditions were the same as recently described.[30] Each sample was injected and analyzed in triplicate. The MS data were recorded with a high resolution Bruker maXis qTOF-MS equipped with an APOLLO II electrospray ion source (Bruker Daltonics, Bremen, Germany), which was operated in electrospray positive mode to achieve maximum compound coverage.[30] Precursor and product ion scans were recorded in a mass range from *m/z* 50 – 1 500 with a scanning rate of 5 Hz. For data-dependent fragmentation, after each precursor scan, the two most abundant precursors were isolated and subjected to collision induced fragmentation. Maximum coverage of MS/MS data was achieved by excluding precursor masses from fragmentation after three successful MS/MS spectra for five minutes. The collision energy was set to 35 eV. All mass spectra were internally calibrated by infusing a tuning mix solution (Agilent Technologies, Waldbronn, Germany) prior to each chromatographic run.

Raw data were post-processed using the XCMS R package (version 3.2.0).[61] Chromatographic features were detected by the *centWave* algorithm[62] using an expected approximate peak width in the range from 10 – 80 s and a maximum tolerated *m/z* deviation of 10 ppm. Retention time alignment was done with the *Orbiwarp* algorithm[63] as integrated in XCMS. Peaks within and between samples then were grouped into chromatographic features (retention time–*m/z*-pairs) based on time dimension densities.[61] In the obtained matrix, only those features were retained, which were reproducibly detected in all three replicate injections of at least one sample.

Data analysis

All further statistical analysis and filtering was done in R Statistical Language and Microsoft Excel 2016. All p-values were calculated based on heteroscedastic Student's t-Tests. The number of double-bond equivalents per carbon atom (DBE/C) and average carbon oxidation state (OS_C) was computed as recently described.[31,56]

Author Contributions

Conceptualization, D.H., M.G., and P.S.-K.; Methodology, D.H., M.G., L.C.P, and P.S.-K.; Investigation, D.H., M.G., L.C.P., and P.S.-K.; Formal Analysis, D.H., M.G., and L.C.P.; Resources, M.G. and P.S.-K.; Writing – Original Draft, D.H.; Writing – Review & Editing, D.H., M.G., L.C.P., J.W.M., M.R., A.J.T., and P.S.-K.; Visualization, D.H.; Supervision, M.G., J.W.M., M.R., A.J.T, and P.S.-K.

Declaration of Interests

The authors declare no competing interests.

J.W.M and A.J.T were employed by Mars Petcare UK while this research was carried out. D.H.'s research is funded by Mars Petcare UK.

References

1. Hellwig M., Henle T. (2014). Baking, Ageing, Diabetes: A Short History of the Maillard Reaction. Angew. Chem. Int. Ed. Engl. *53*, 10316–10329.
2. Yaylayan V.A. (2003). Recent Advances in the Chemistry of Strecker Degradation and Amadori Rearrangement. Food Sci. Technol. Res. *9*, 1–6.
3. Henning C., Glomb M.A. (2016). Pathways of the Maillard reaction under physiological conditions. Glycoconj. J. *33*, 499–512.
4. Wang H.-Y., Qian H., Yao W.-R. (2011). Melanoidins produced by the Maillard reaction: Structure and biological activity. Food Chem. *128*, 573–584.
5. Lindenmeier M., Faist V., Hofmann T. (2002). Structural and Functional Characterization of Pronyl-lysine, a Novel Protein Modification in Bread Crust Melanoidins Showing in Vitro Antioxidative and Phase I/II Enzyme Modulating Activity. J. Agric. Food Chem. *50*, 6997–7006.
6. Hofmann T. (1998). Studies on the Relationship between Molecular Weight and the Color Potency of Fractions Obtained by Thermal Treatment of Glucose/Amino Acid and Glucose/Protein Solutions by Using Ultracentrifugation and Color Dilution Techniques. J. Agric. Food Chem. *46*, 3891–3895.

7. Davies M.J., Truscott R.J.W. (2001). Photo-oxidation of proteins and its role in cataractogenesis. J. Photochem. Photobiol. B *63*, 114–125.

8. Bensasson R.V., Land E.J., Truscott T.G. (1983). Flash Photolysis and Pulse Radiolysis: Contributions to the Chemistry of Biology and Medicine (Elsevier Science).

9. Papeschi G., Monici M., Pinzauti S. (1982). pH effect on dye sensitized photooxygenation of amino acids and albumins. Med. Biol. Environ. *10*, 245–250.

10. Nagaraj R.H., Monnier V.M. (1992). Isolation and characterization of a blue fluorophore from human eye lens crystallins. Biochim. Biophys. Acta General Subjects *1116*, 34–42.

11. de La Rochette A., Birlouez-Aragon I., Silva E., Morlière P. (2003). Advanced glycation endproducts as UVA photosensitizers of tryptophan and ascorbic acid. Biochim. Biophys. Acta General Subjects *1621*, 235–241.

12. Wondrak G.T., Roberts M.J., Jacobson M.K., Jacobson E.L. (2002). Photosensitized Growth Inhibition of Cultured Human Skin Cells. J. Invest. Dermatol. *119*, 489–498.

13. Argirova M.D., Breipohl W. (2002). Glycated Proteins Can Enhance Photooxidative Stress in Aged and Diabetic Lenses. Free Radic. Res. *36*, 1251–1259.

14. Linetsky M., Ortwerth B.J. (1996). Quantitation of the Reactive Oxygen Species Generated by the UVA Irradiation of Ascorbic Acid-Glycated Lens Proteins. Photochem. Photobiol. *63*, 649–655.

15. Ortwerth B.J., Malladi P., H N.R., Mikhail L. (1997). The Relative UV Sensitizer Activity of Purified Advanced Glycation Endproducts. Photochem. Photobiol. *65*, 666–672.

16. Wondrak G.T., Jacobson E.L., Jacobson M.K. (2002). Photosensitization of DNA damage by glycated proteins. Photochem. Photobiol. Sci. *1*, 355–363.

17. Hellwig M., Gensberger-Reigl S., Henle T., Pischetsrieder M. (2018). Food-derived 1,2-dicarbonyl compounds and their role in diseases. Semin. Cancer Biol. *49*, 1-8.

18. Encinas M.V., Rufs A.M., Lissi E.A. (1985). Photochemistry of hydroxyalkanones in solution. J. Chem. Soc., Perkin Trans. 2, 457–460.

19. Lebedeva N.V., Chen T.K., Forbes M.D.E. (2010). Solvent- and Wavelength-Dependent Photochemistry of 1,3-Dihydroxyacetone Studied by TREPR. Appl. Magn. Reson. *38*, 155–166.

20. Steenken S., Jaenicke-Zauner W., Schulte-Frohlinde D. (1975). Photofragmentation of hydroxyacetone, 1.3-dihydroxyacetone, and 1.3-dicarboxyacetone in aqueous solution. An EPR study. Photochem. Photobiol. *21*, 21–26.

21. Bohart G.S., Carson J.F. (1955). Effects of Trace Metals, Oxygen and Light on the Glucose–Glycine Browning Reaction. Nature *175*, 470–471.

22. Kessel L., Kalinin S., Soroka V., Larsen M., Johansson L.B.-Å. (2005). Impact of UVR-A on whole human lenses, supernatants of buffered human lens homogenates, and purified argpyrimidine and 3-OH-kynurenine. Acta Ophthalmol. *83*, 221–227.

23. Baisier W.M., Labuza T.P. (1992). Maillard browning kinetics in a liquid model system. J. Agric. Food Chem. *40*, 707–713.

24. Morales F.J., van Boekel M.A.J.S. (1998). A Study on Advanced Maillard Reaction in Heated Casein/Sugar Solutions. Int. Dairy J. *8*, 907–915.

25. Matiacevich S.B., Santagapita P.R., Buera M.P. (2005). Fluorescence from the Maillard Reaction and its Potential Applications in Food Science. Crit. Rev. Food Sci. Nutr. *45*, 483–495.

26. Graham L., Nagaraj R.H., Sayre L.M., Monnier V.M. (1998). Structure and Biological Significance of Pentodilysine, a Novel Fluorescent Advanced Maillard Reaction Protein Crosslink. In The Maillard Reaction in Foods and Medicine, J. O'Brien, H.E. Nursten, M.J. Crabbe, J.M. Ames, ed. (Elsevier Reference Monographs), p. 410.

27. Graham L. (1996). A comprehensive survey of the acid-stable fluorescent cross-links formed by ribose with basic amino acids, and partial characterization of a novel Maillard cross-link. Biochim. Biophys. Acta Protein Structure and Molecular Enzymology *1297*, 9–16.

28. Shipanova I.N., Glomb M.A., Nagaraj R.H. (1997). Protein Modification by Methylglyoxal. Arch. Biochem. Biophys. *344*, 29–36.

29. Murphy K.R., Stedmon C.A., Graeber D., Bro R. (2013). Fluorescence spectroscopy and multi-way techniques. PARAFAC. Anal. Methods *5*, 6557–6566.

30. Hemmler D., Heinzmann S.S., Wöhr K., Schmitt-Kopplin P., Witting M. (2018). Tandem HILIC-RP liquid chromatography for increased polarity coverage in food analysis. Electrophoresis *39*, 1645–1653.

31. Hemmler D., Roullier-Gall C., Marshall J.W., Rychlik M., Taylor A.J., Schmitt-Kopplin P. (2017). Evolution of Complex Maillard Chemical Reactions, Resolved in Time. Sci. Rep. *7*, 3227.

32. Davies M.J. (2005). The oxidative environment and protein damage. Biochim. Biophys. Acta Proteins and Proteomics *1703*, 93–109.

33. Pattison D.I., Rahmanto A.S., Davies M.J. (2012). Photo-oxidation of proteins. Photochem. Photobiol. Sci. *11*, 38–53.

34. Agon V.V., Bubb W.A., Wright A., Hawkins C.L., Davies M.J. (2006). Sensitizer-mediated photooxidation of histidine residues. Free Radic. Biol. Med. *40*, 698–710.

35. Chang S.H., Teshima G.M., Milby T., Gillece-Castro B., Canova-Davis E. (1997). Metal-catalyzed photooxidation of histidine in human growth hormone. Anal. Biochem. *244*, 221–227.

36. Tomita M., Irie M., Ukita T. (1969). Sensitized photooxidation of histidine and its derivatives. Products and mechanism of the reaction. Biochemistry *8*, 5149–5160.

37. Sjöberg B., Foley S., Staicu A., Pascu A., Pascu M., Enescu M. (2016). Protein reactivity with singlet oxygen. J. Photochem. Photobiol. B *159*, 106–110.

38. Wilkinson F., Helman W.P., Ross A.B. (1995). Rate Constants for the Decay and Reactions of the Lowest Electronically Excited Singlet State of Molecular Oxygen in Solution. An Expanded and Revised Compilation. J. Phys. Chem. Ref. Data *24*, 663–677.

39. Kai S., Suzuki S. (1996). Dye-sensitized Photooxidation of 2,4-Disubstituted Imidazoles: The Formation of Isomeric Imidazolinones. Heterocycles *43*, 1185–1188.

40. Michaeli A., Feitelson J. (1994). Reactivity of singlet oxygen toward amino acids and peptides. Photochem. Photobiol. *59*, 284–289.

41. Miskoski S., Garcia N.A. (1993). Influence of the peptide bond on the singlet molecular oxygen-mediated (O21 delta g) photooxidation of histidine and methionine dipeptides. A kinetic study. Photochem. Photobiol. *57*, 447–452.

42. Gomyo T., Yang Y., Fujimaki M. (1968). Comparision of Photosensitizing Ability of Dyes in Oxidation of Histidine. Agric. Biol. Chem. *32*, 1061–1069.

43. Liu F., Lu W., Fang Y., Liu J. (2014). Evolution of oxidation dynamics of histidine. Phys. Chem. Chem. Phys. *16*, 22179–22191.

44. Hwang S.H., Wang Z., Suh H.-W., Lim S.S. (2018). Antioxidant activity and inhibitory effects of 2-hydroxy-3-methylcyclopent-2-enone isolated from ribose–histidine Maillard reaction products on aldose reductase and tyrosinase. Food Funct. *9*, 1790–1799.

45. Yilmaz Y., Toledo R. (2005). Antioxidant activity of water-soluble Maillard reaction products. Food Chem. *93*, 273–278.

46. Hayase F., Koyama T., Konishi Y. (1997). Novel Dehydrofuroimidazole Compounds Formed by the Advanced Maillard Reaction of 3-Deoxy-d-hexos-2-ulose and Arginine Residues in Proteins. J. Agric. Food Chem. *45*, 1137–1143.

47. Morales F.J., Babbel M.-B. (2002). Antiradical Efficiency of Maillard Reaction Mixtures in a Hydrophilic Media. J. Agric. Food Chem. *50*, 2788–2792.

48. Vistoli G., De Maddis D., Cipak A., Zarkovic N., Carini M., Aldini G. (2013). Advanced glycoxidation and lipoxidation end products (AGEs and ALEs): an overview of their mechanisms of formation. Free Radic. Res. *47*, 3–27.

49. Hellwig M., Henle T. (2010). Formyline, a new glycation compound from the reaction of lysine and 3-deoxypentosone. Eur. Food. Res. Technol. *230*, 903–914.

50. Lederer M.O., Klaiber R.G. (1999). Cross-linking of proteins by maillard processes. Bioorg. Med. Chem. *7*, 2499–2507.

51. Hodge J.E. (1953). Dehydrated Foods, Chemistry of Browning Reactions in Model Systems. J. Agric. Food Chem. *1*, 928–943.

52. Karstens T., Rossbach V. (1989). Thermo-oxidative degradation of polyamide 6 and 6,6. Kinetics of the formation and inhibition of UV/VIS-active chromophores. Macromol. Chem. Phys. *190*, 3033–3053.

53. Moritz F., Kaling M., Schnitzler J.-P., Schmitt-Kopplin P. (2017). Characterization of poplar metabotypes via mass difference enrichment analysis. Plant Cell Environ. *40*, 1057–1073.

54. Moritz F., Janicka M., Zygler A., Forcisi S., Kot-Wasik A., Kot J., Gebefügi I., Namiesnik J., Schmitt-Kopplin P. (2015). The compositional space of exhaled breath condensate and its link to the human breath volatilome. J. Breath Res. *9*, 27105.

55. Hertkorn N., Frommberger M., Witt M., Koch B.P., Schmitt-Kopplin P., Perdue E.M. (2008). Natural Organic Matter and the Event Horizon of Mass Spectrometry. Anal. Chem. *80*, 8908–8919.

56. Hemmler D., Roullier-Gall C., Marshall J.W., Rychlik M., Taylor A.J., Schmitt-Kopplin P. (2018). Insights into the Chemistry of Non-Enzymatic Browning Reactions in Different Ribose-Amino Acid Model Systems. Sci. Rep. *8*, 16879.

57. Aiona P.K., Luek J.L., Timko S.A., Powers L.C., Gonsior M., Nizkorodov S.A. (2018). Effect of Photolysis on Absorption and Fluorescence Spectra of Light-Absorbing Secondary Organic Aerosols. ACS Earth Space Chem. *2*, 235–245.

58. Timko S.A., Gonsior M., Cooper W.J. (2015). Influence of pH on fluorescent dissolved organic matter photo-degradation. Water Res. *85*, 266–274.

59. Kanawati B., Bader T.M., Wanczek K.-P., Li Y., Schmitt-Kopplin P. (2017). Fourier transform (FT)-artifacts and power-function resolution filter in Fourier transform mass spectrometry. Rapid Commun. Mass Spectrom. *31*, 1607–1615.

60. Lucio M., Fekete A., Frommberger M., Schmitt-Kopplin P. (2011). Metabolomics: High-Resolution Tools Offer to Follow Bacterial Growth on a Molecular Level. In Handbook of Molecular Microbial Ecology I: Metagenomics and Complementary Approaches, F.J. de Bruijn, ed. (John Wiley & Sons, Inc), pp. 683–695.

61. Smith C.A., Want E.J., O'Maille G., Abagyan R., Siuzdak G. (2006). XCMS: Processing Mass Spectrometry Data for Metabolite Profiling Using Nonlinear Peak Alignment, Matching, and Identification. Anal. Chem. *78*, 779–787.

62. Tautenhahn R., Böttcher C., Neumann S. (2008). Highly sensitive feature detection for high resolution LC/MS. BMC Bioinform. *9*, 504.

63. Prince J.T., Marcotte E.M. (2006). Chromatographic Alignment of ESI-LC-MS Proteomics Data Sets by Ordered Bijective Interpolated Warping. Anal. Chem. *78*, 6140–6152.

Sunlight selectively modifies Maillard reaction products in a wide array of chemical reactions

Daniel Hemmler[1,2]*, Michael Gonsior[3], Leanne C. Powers[3], James W. Marshall[4], Michael Rychlik[1], Andrew J. Taylor[4], and Philippe Schmitt-Kopplin[1,2,3]*

SUPPORTING INFORMATION

Author affiliations

[1]*Comprehensive Foodomics Platform, Analytical Food Chemistry, Technical University Munich, Maximus-von-Imhof-Forum 2, 85354 Freising, Germany.*

[2]*Research Unit Analytical BioGeoChemistry (BGC), Helmholtz Zentrum München, Ingolstädter Landstrasse 1, 85764 Neuherberg, Germany.*

[3]*University of Maryland Center for Environmental Science, Chesapeake Biological Laboratory, Solomons, USA.*

[4]*The Waltham Centre for Pet Nutrition, Mars Petcare UK, Waltham-on-the-Wolds, Leicestershire, LE14 4RT, United Kingdom.*

Corresponding authors

Philippe Schmitt-Kopplin

Research Unit Analytical BioGeoChemistry (BGC), Helmholtz Zentrum München, Ingolstädter Landstrasse 1, 85764 Neuherberg, Germany.

Phone: +49 89 3187 3246

E-Mail: schmitt-kopplin@helmholtz-muenchen.de

Daniel Hemmler

Comprehensive Foodomics Platform, Analytical Food Chemistry, Technical University Munich, Alte Akademie 10, 85354 Freising, Germany.

Phone: +49 89 3187 2216

E-Mail: daniel.hemmler@tum.de

Holistic characterization of photosensitive MRPs

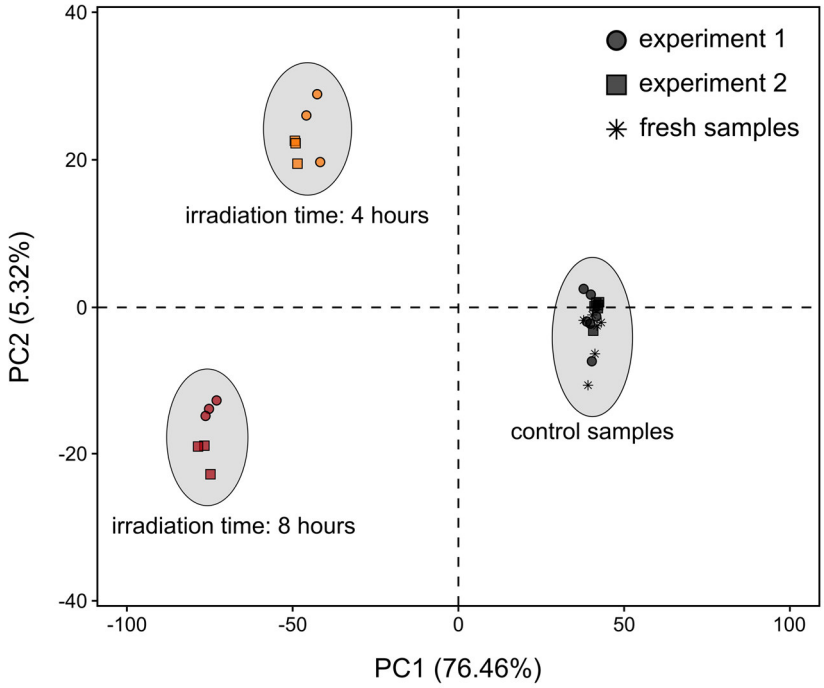

Figure S1. Principal Component analysis of ribose-histidine FT-ICR-MS raw data. Samples were irradiated for four and eight hours in a suntester system. Additionally, control samples, which were kept under same conditions, however, protected from light exposure, as well as freshly prepared model systems were analyzed. All experiments were carried out in two independent experiments. Each sample was further injected in triplicate measurements (total number of samples per treatment = 6). Samples and replicate injections were measured in randomized order.

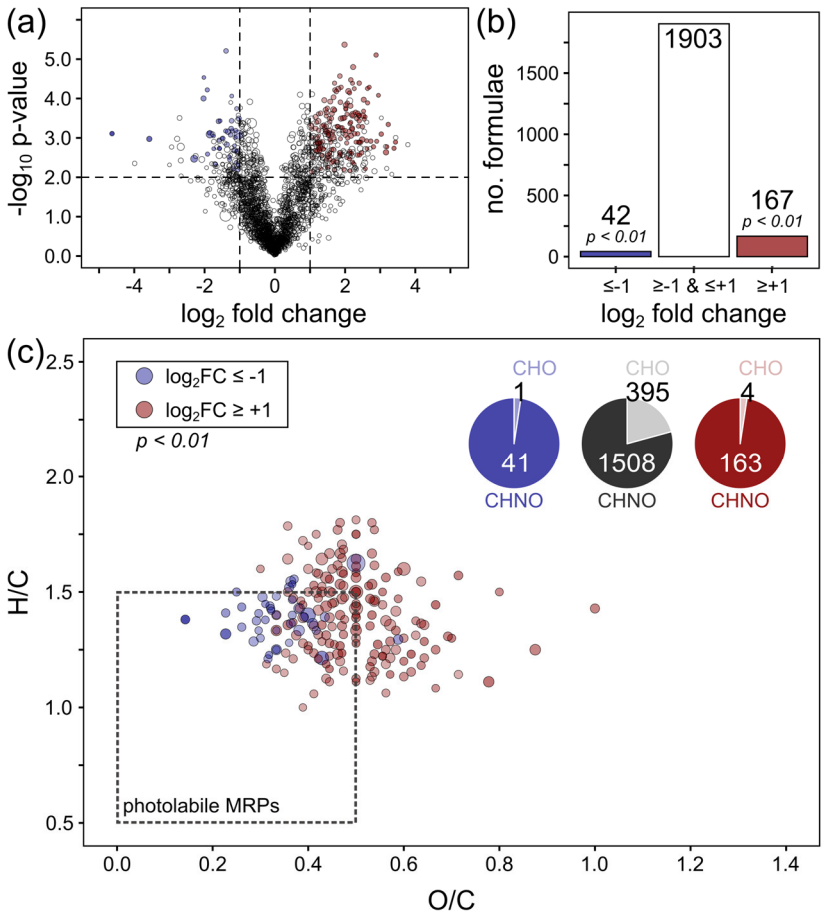

Figure S2. Effect of solar irradiation on elemental compositions of **ribose-lysine MRPs**. Model systems were irradiated for eight hours and compared to unirradiated control samples. Irradiation experiments were performed in duplicate. Each sample then was analyzed by FT-ICR-MS in triplicate injections (N = 2 × 3). Peak intensities of all features found in irradiated samples were compared to the same features in the unirradiated control samples by Student's t-Test (n = 3): Features, which showed a significant decrease in peak intensities in both independent irradiation experiments are colored in blue. Features, which showed a significant increase or were newly formed upon irradiation are highlighted in red, respectively. Volcano plot **(a)**. Number of molecular formulae showing significant changes in peak intensities **(b)**. Van Krevelen diagram of all significantly affected molecular formulae **(c)**. Pie charts illustrate the reduced occurrence of nitrogen-free (CHO) MRPs in photochemical reactions. Black pie chart represents elemental compositions, which did not show a significant change in peak intensities upon irradiation.

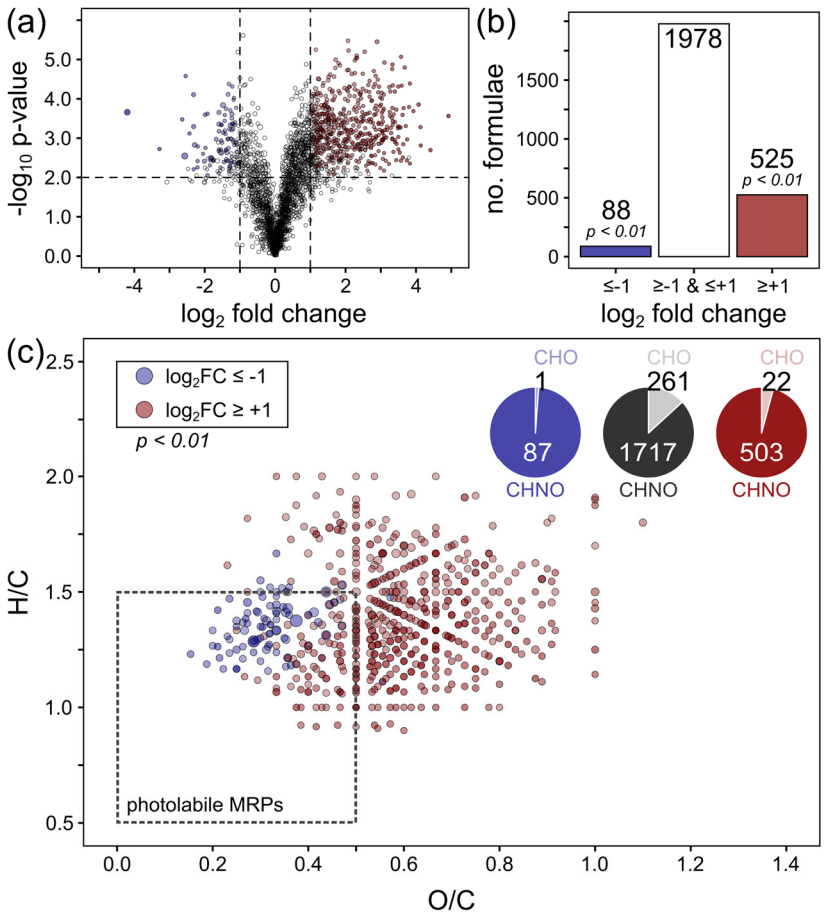

Figure S3. Effect of solar irradiation on elemental compositions of **ribose-arginine MRPs**. Model systems were irradiated for eight hours and compared to unirradiated control samples. Irradiation experiments were performed in duplicate. Each sample then was analyzed by FT-ICR-MS in triplicate injections (N = 2 × 3). Peak intensities of all features found in irradiated samples were compared to the same features in the unirradiated control samples by Student's t-Test (n = 3): Features, which showed a significant decrease in peak intensities in both independent irradiation experiments are colored in blue. Features, which showed a significant increase or were newly formed upon irradiation are highlighted in red, respectively. Volcano plot **(a)**. Number of molecular formulae showing significant changes in peak intensities **(b)**. Van Krevelen diagram of all significantly affected molecular formulae **(c)**. Pie charts illustrate the reduced occurrence of nitrogen-free (CHO) MRPs in photochemical reactions. Black pie chart represents elemental compositions, which did not show a significant change in peak intensities upon irradiation.

Photooxidation of MRPs by singlet oxygen

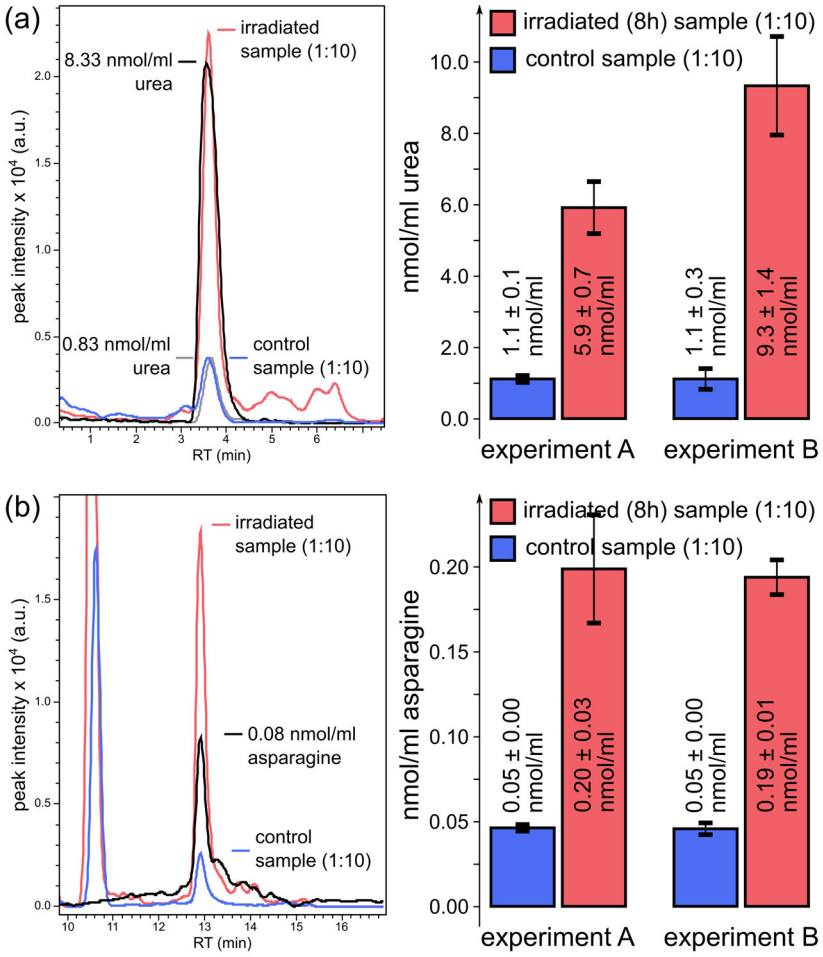

Figure S4. Quantification of urea **(a)** and asparagine **(b)** in ribose-histidine model systems. After lyophilization, the model systems were reconstituted in 2% acetonitrile solution to achieve a dilution factor of 1:10 (*v/v*) with respect to the original model system. Calibration curves were computed from analyzed standard solutions as shown below.

Calibration standards used for quantification of urea and asparagine in ribose-histidine model systems. Standards were prepared in 2% acetonitrile solution. Concentration values are given in nmol ml^{-1}.

calibrant	urea	L-asparagine
1	0.08	0.04
2	0.17	0.08
3	0.83	0.38
4	1.67	0.76
5	8.33	3.78
6	16.65	

The role of imidazole groups in photochemical reactions

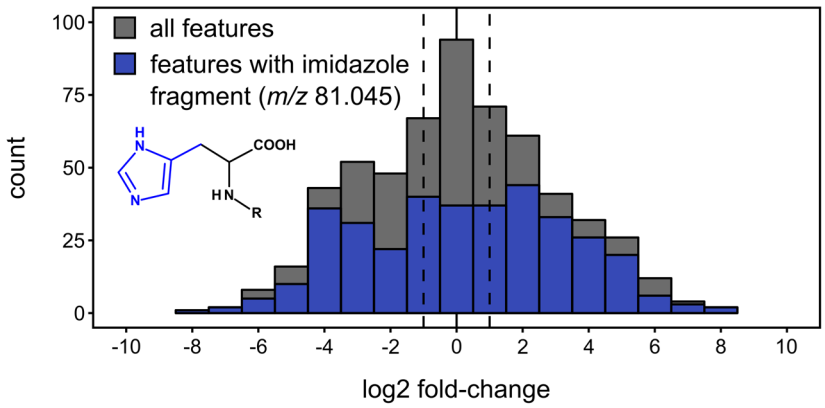

Figure S5. Screening of fragment spectra containing imidazole fragment *m/z* = 81.045. Fragment spectra were acquired by data-dependent LC-MS/MS. Histograms illustrate the log2 fold change (irradiated samples vs. control samples) of the peak intensities as influenced by irradiating ribose-histidine samples for eight hours. Gray histogram represents all chromatographic features with available MS/MS spectra (N = 580). Blue histogram shows only features, which contained an imidazole characteristic fragment (*m/z* = 81.045) in their MS/MS spectra (N = 355).

Chemical diversity of thermally formed MRPs

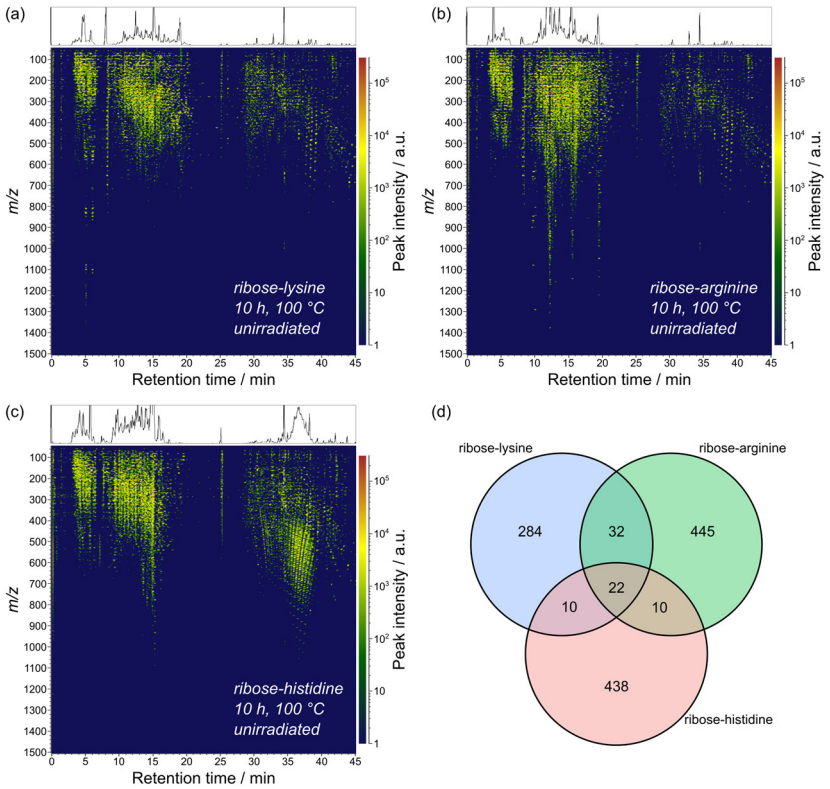

Figure S6. Non-target analysis of unirradiated model systems by tandem HILIC-RP chromatography. Retention time versus *m/z*-value plots of a ribose-lysine (a), ribose-arginine (b), and ribose-histidine (c) model system, heated for ten hours at 100 °C. Each dot in (a-c) represents an analytical signal (feature) colored according to the observed peak intensity. Venn diagram illustrates the amino acid specific chemical diversity in produced MRPs (d). Between the three model systems, chromatographic features were considered as the same chemical compound when m/z-values and retention times were equal (*m/z*-alignment: ± 10 ppm and ΔRT ≤ 30 s).

Compositional description of antioxidants

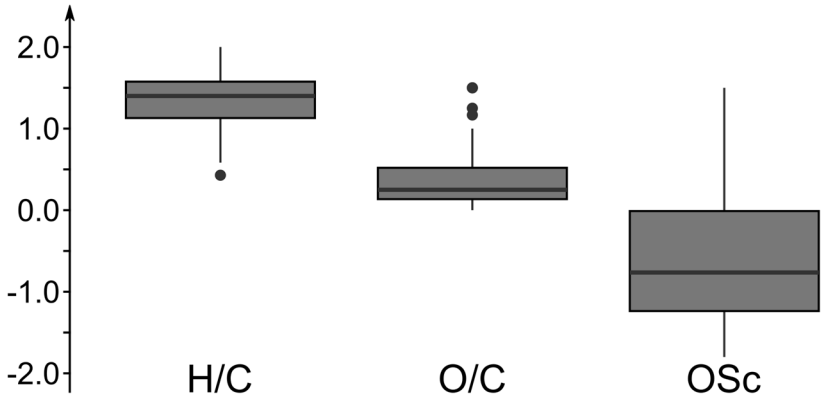

Figure S7. Compositional descriptors retrieved for 125 antioxidants containing no more than C, H, N, and O elements. Antioxidants were taken from FooDB (Release June 29, 2017).

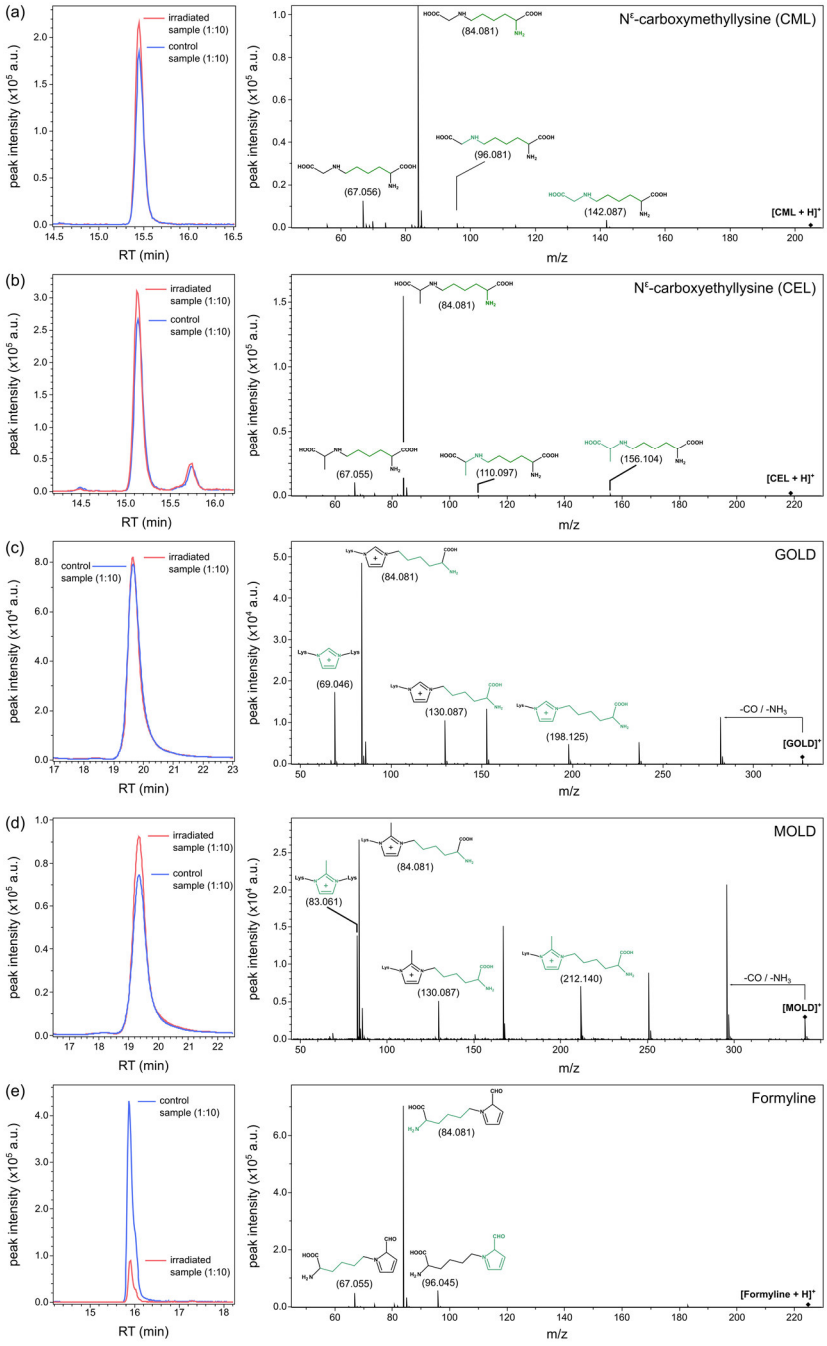

Figure S8. LC-MS/MS analysis of AGE markers in unirradiated ribose-lysine model systems (blue) and ribose-lysine model systems irradiated for eight hours (red). Structures were confirmed by MS/MS spectra. Analyzed markers were: carboxymethyllyine (CML) (a), carboxyethyllysine (CEL) (b), GOLD (c), MOLD (d), and formyline (e).

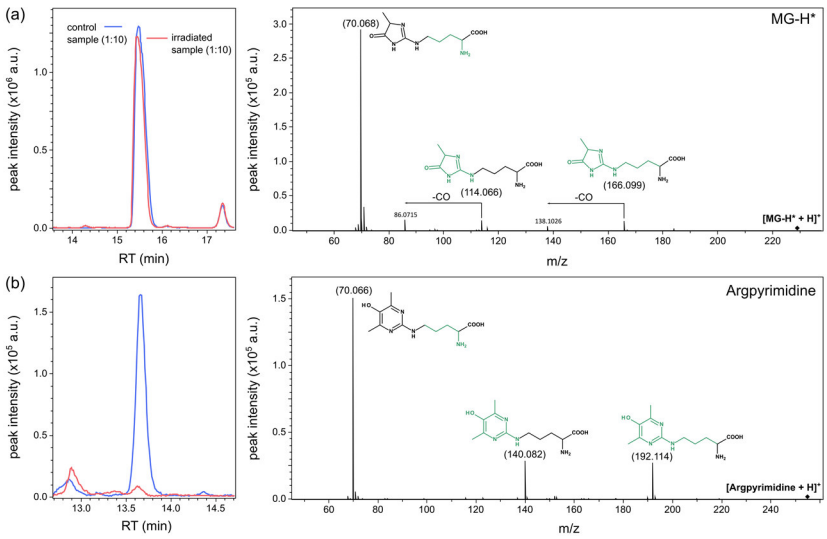

Figure S9. LC-MS/MS analysis of AGE markers in unirradiated ribose-arginine model systems (blue) and ribose-arginine model systems irradiated for eight hours (red). Structures were confirmed by MS/MS spectra. Analyzed markers were: one hydroimidazolone isomer MG-H* (assignment of the three possible isomers MG-H1 – MG-H3 based on MS/MS data not possible) (a), and argpyrimidine (b).

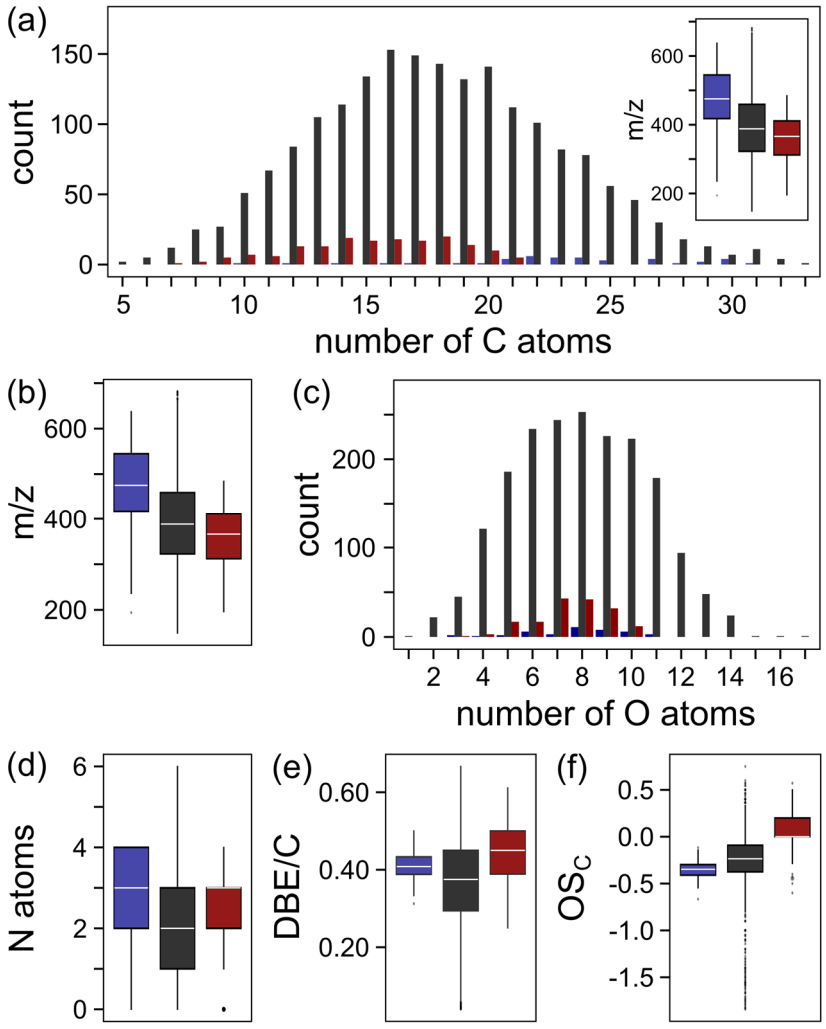

Figure S10. Overview of compositional descriptors retrieved for the **ribose-lysine** model system after molecular formulae computation from FT-ICR-MS data. Bar charts are grouped into features, which showed a significant decrease (blue; log2FC < -1 and $p < 0.01$, Student's t-Test (n = 3)) and significant increase (red; log2FC > 1 and $p < 0.01$, Student's t-Test (n = 3)) in peak intensities in both independent irradiation experiments, respectively. Features that did not show a significant change in peak intensities after an irradiation time of eight hours are colored in dark gray. Represented descriptors are number of carbon atoms per formula **(a)**, measured *m/z*-values **(b)**, number of oxygen **(c)**, and number of nitrogen atoms per formula **(d)**, as well as average number of double bond equivalents per carbon atom **(e)** and average carbon oxidation state **(f)**.

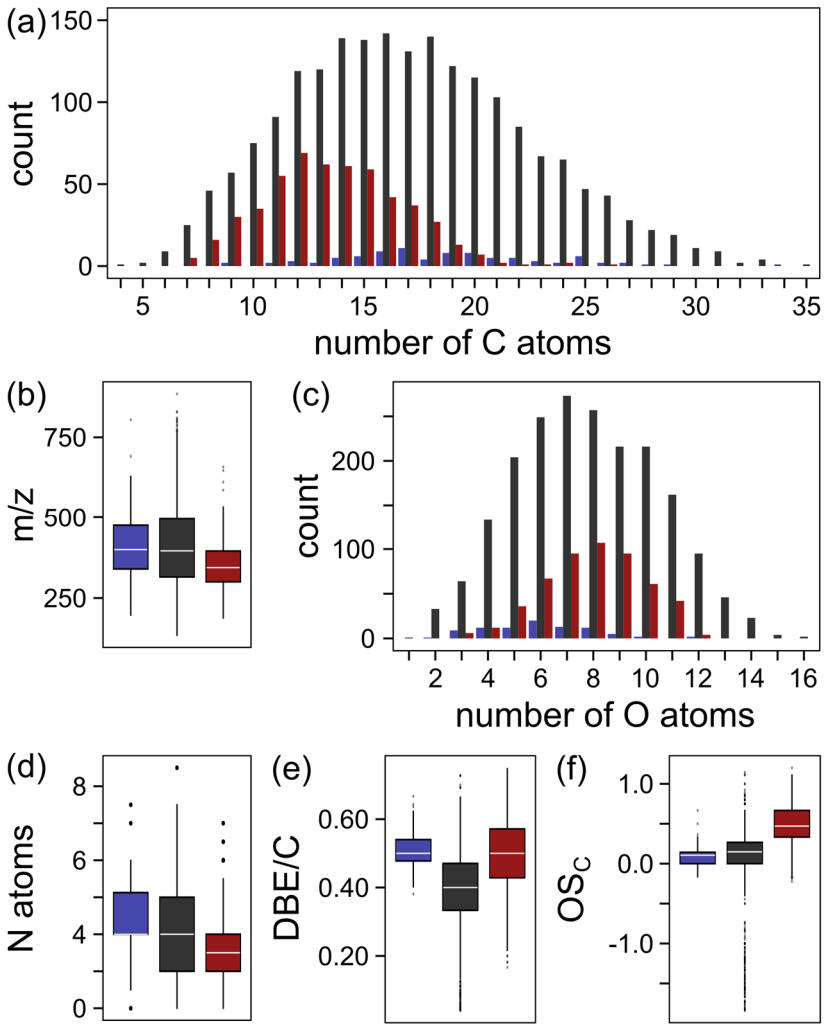

Figure S11. Overview of compositional descriptors retrieved for the **ribose-arginine** model system after molecular formulae computation from FT-ICR-MS data. Bar charts are grouped into features, which showed a significant decrease (blue; log2FC < -1 and p < 0.01, Student's t-Test (n = 3)) and significant increase (red; log2FC > 1 and p < 0.01, Student's t-Test (n = 3)) in peak intensities in both independent irradiation experiments, respectively. Features that did not show a significant change in peak intensities after an irradiation time of eight hours are colored in dark gray. Represented descriptors are number of carbon atoms per formula **(a)**, measured *m/z*-values **(b)**, number of oxygen **(c)**, and number of nitrogen atoms per formula **(d)**, as well as average number of double bond equivalents per carbon atom **(e)** and average carbon oxidation state **(f)**.

Changes in pH during irradiation experiments

Table S1. Measured pH values during irradiation of Maillard model systems in the custom-built photolysis system used for online EEM measurements.

Irradiation time	pH ribose-lysine	pH ribose-arginine	pH ribose-histidine
0 h (before irradiation)	6.06	6.64	6.01
4 h	5.48	6.29	5.64
8 h	5.30	6.14	5.48
12 h	5.19	6.10	5.42
16 h	5.14	6.07	5.38
20 h	5.10	6.07	5.37

Table S2. Measured pH values (mean from n = 2 irradiation experiments) before and after irradiation of Maillard model systems in the Suntest CPS system.

Irradiation time	pH ribose-lysine	pH ribose-arginine	pH ribose-histidine
0 h (before irradiation)	6.0	6.6	6.0
8 h (after irradiation)	5.2	6.1	5.4